Structural change induced in TiO_2 by swift heavy ions and its application to three-dimensional lithography

Ken-ichi Nomura, Tetsuya Nakanishi, Yoshihiro Nagasawa, and Yoshimichi Ohki
Department of Electrical, Electronics and Computer Engineering, Waseda University, Shinjuku, Tokyo 169-8555, Japan

Koichi Awazu,* Makoto Fujimaki, and Naoto Kobayashi
Photonic Research Institute, National Institute of Advanced Industrial Science and Technology, Tsukuba Central 4, Tsukuba 305-8562, Japan

Satoshi Ishii and Kunihiro Shima
Tandem Accelerator Center, University of Tsukuba, Tsukuba 305-8577, Japan
(Received 14 March 2003; published 8 August 2003)

A rutile TiO_2 single crystal was irradiated by heavy ions with a high energy of the order of several tens of MeV. A good etching selectivity, where only the irradiated surface is well etched by hydrofluoric acid is induced by the irradiation. Through x-ray diffraction and high-resolution electron microscopy, it became clear that the irradiated region lost crystallization. It is considered that this amorphous region and the surrounding region are dissolved in hydrofluoric acid. Through the calculation of the ion energy, it was found that the etching always stopped at the depth where the electronic stopping power of the ion decayed to a critical value of 6.2 keV/nm, regardless of the ion species in the case of I, Br, Cu, and Ti ions. However, in the case of Ca ions with energies higher than about 72 MeV or Cl ions with energies higher than about 77 MeV, the irradiated top surface was not etched with hydrofluoric acid, but the inside surface several μm deep from the irradiated surface was etched. A calculation shows that the critical factor which determines whether the irradiated surface can be etched or not is the lateral energy density on the surface deposited by ions. The etched surface observed by atomic force microscopy is very smooth with a roughness of the order of nm. Therefore, a combination of ion irradiation and etching can be used as a novel fabrication method of nanostructures in rutile.

DOI: 10.1103/PhysRevB.68.064106 PACS number(s): 61.80.Jh, 61.72.Ff, 34.50.Bw, 85.40.Hp

I. INTRODUCTION

Titanium dioxide (TiO_2), which has three crystalline polymorphs—rutile, anatase, and brookite—is attracting much attention due to its versatile application possibilities, such as rutile semiconductor-electrolyte interfaces for photocatalysts[1–3] and solar cells.[4,5] Rutile TiO_2 single crystal, hereafter abbreviated as rutile, with a large birefringence and an excellent chemical resistance has wide potentialities in the fields of integrated optics and photonic devices. Titanium dioxide with a low optical loss at wavelengths in the vicinity of 1.5 μm can be used as a dopant for a planar optical waveguide for optical communication.[6–9] Amorphous TiO_2 with optical band gap at 3 eV is also available as a coating material for a window of Hg and Xe arc lamps.[10]

A new paradigm emerged in the past decade, in which the band-structure concept of solid-state physics is applied to radio,[11] microwave,[12] and optical waves.[13] This has led to the invention of photonic crystal structures in two or three dimensions,[14] which can be applied for outstanding optical devices for controlling electromagnetic waves such as a superprism,[15,16] sharp-bend optical waveguide,[17] and high-Q cavity.[18] Among numerous possible materials for photonic devices, semiconductors such as silicon, GaAs, and InP have been most examined because of the abundant knowledge of microfabrication.[19,20] However, their refractive index values—e.g., 3.5 for silicon—are higher than 1.45 for silica,[21,22] resulting in a high connection loss between the photonic crystal and silica-based optical waveguide. Their band gaps are too small to make photonic crystals for visible light. Compared to these materials, the refractive index of rutile—2.4 perpendicular to the c axis or 2.7 parallel[23]—is close to silica. Furthermore, its band gap is as wide as 3.0 eV (Ref. 10) and its optical transmission loss is 10 times lower than that of silicon at wavelengths near 1.5 μm.[24] For these reasons, rutile TiO_2 has a high potentiality for a photonic crystal.

In order to use rutile for integrated optics, photonic devices, and photonic crystals, a proper micro-fabrication or nanofabrication process must be developed. Reactive ion etching cannot be used, since the fabricated side wall is not smooth enough to be used for photonic[25,26] such as an arrayed waveguide grating. Furthermore, a proper etching gas for rutile is not known. Although the sol-gel method[27,28] was used to fabricate an artificial opal structure of TiO_2,[29] shrinkage and cracking of the gel are unavoidable.

Since 2000, the authors have shown examples of nanofabrication using swift heavy ions.[30] When a swift heavy ion passes through most insulators, its energy is reduced while creating a heavily damaged zone along its path. The damaged zone can be made visible by chemical etching: thus the ion path and visible track are called the ''latent track'' and ''etched track,'' respectively. In many solid materials such as amorphous SiO_2 generation of etched tracks has been reported.[30] The sidewall of the etched track is very flat with a roughness of only a few nm.[25–27] Most of the earlier studies on that are concerned with identification of both particle species and their energy by observation of the etched track

 ©2003 The American Physical Society

diameter, made possible by the chemical etch rate along a particle track dependents on projectile mass.[31] Other studies have focused on the very early stages of track formation and how excited electrons transfer energy to the network. The thermal spike model[32] is one of the most widely accepted theories for describing how ion energy is transferred rapidly and locally, introducing extremely high temperatures along the ion path. However, the model gives little information on the structure of the latent track and on the atomic mechanism underlying the enhanced etch rate of the latent track. In the present study, we attempt to improve our understanding of these latter issues by approaching the problem from different angles, correlating the changes of x-ray diffraction (XRD), atomic force microscopy (AFM), scanning electron microscopy (SEM), and high-resolution transmission electron microscopy (HREM). We chose TiO_2 rutile single crystal to examine the defects generated in the particle tracks in order to develop three-dimensional fabrication with nm flatness, yet the structure of the latent track and the mechanism underlying the generation of latent tracks in these materials have not been investigated. The threshold ion energy necessary for fabrication is also discussed.

II. EXPERIMENTAL PROCEDURES

The samples used in the present experiment are rutile TiO_2 single crystals (purity$>$99.99%, density 4.25 g/cm^3) synthesized by the Verneuil flame-fusion method. For most experiments, crystals with (100) faces were used, while those with (111) and (001) faces were also used to examine the effect of crystal orientation. Unless otherwise stated, the results obtained for the (100) crystal will be described. The samples were cut into plates 500 μm thick and polished. The root-mean-square roughness of the polished surface estimated by AFM is less than 0.8 nm.

Ion irradiation using a 12-MV tandem accelerator at the Tandem Accelerator Center, University of Tsukuba (UTTAC) was performed at room temperature in a vacuum with a residual pressure below 1×10^{-3} Pa. The ions were irradiated to the sample either directly or through a free-standing aluminum or gold foil in order to diffuse them and to lower their energy. The structural change induced by ion irradiation was examined by XRD with a Rigaku FR-MDG spectrometer. The sample surface was observed by SEM, Hitachi S-2500CX and HREM, Hitachi H-9000NAR in addition to AFM. Chemical etching was performed with a hydrofluoric acid (HF) solution of 20% at room temperature.

III. RESULTS

First, the etching rate of the rutile (100) crystal that had not been irradiated by ions was measured. Half of the rutile surface was covered with polytetrafluoroethylene tape and was etched with the HF solution for 7 days. No step was found by a profilometer with a resolution of several nm between the covered and noncovered regions, which means that rutile is not etched by HF.

Figure 1 shows an AFM image of the rutile surface irradiated by Br ions with an energy of 120 MeV to a dose of 8.0×10^{13} cm^{-2} through a 13-μm-thick gold stencil mask with a two-dimensional array pattern of square-shaped holes of 32×32 μm^2. It is observed that the irradiated parts swelled due to expansion of the volume. The height of the step induced by the swelling increases with an increase in the irradiated dose until it reaches a saturation value H shown in Table I. Part of the surface of another rutile sample was covered by a clearly cut silicon single-crystal wafer and irradiated by 110-MeV Cu ions to a dose of 8.0×10^{13} cm^{-2}. Figure 2(a) shows a SEM image of the surface after being

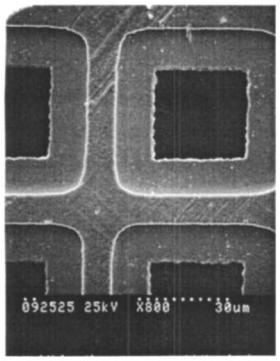

(a)

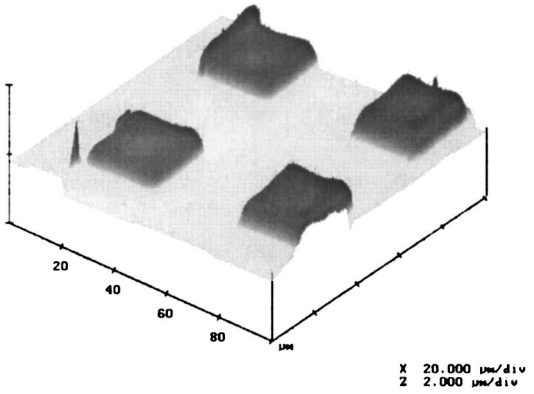

(b)

FIG. 1. (a) SEM observation of the stencil mask made of gold with square-shaped holes. (b) An AFM image of the rutile surface irradiated by 120-MeV Br ions to a dose of 8.0×10^{13} cm^{-2} through a gold mask with square-shaped holes.

TABLE I. Saturation values of the height of swollen surface H induced by ion irradiation and the etched depth D_s.

Ion species	Energy [MeV]	H [μm]	D_s [μm]
I	78.8	0.5	4.6
Br	120	0.9	8.1
	50	0.4	4.0
Cu	110	0.9	8.1
	84.5	0.7	6.3
	15	0.1	0.9
Ti	100	1.0	9.6

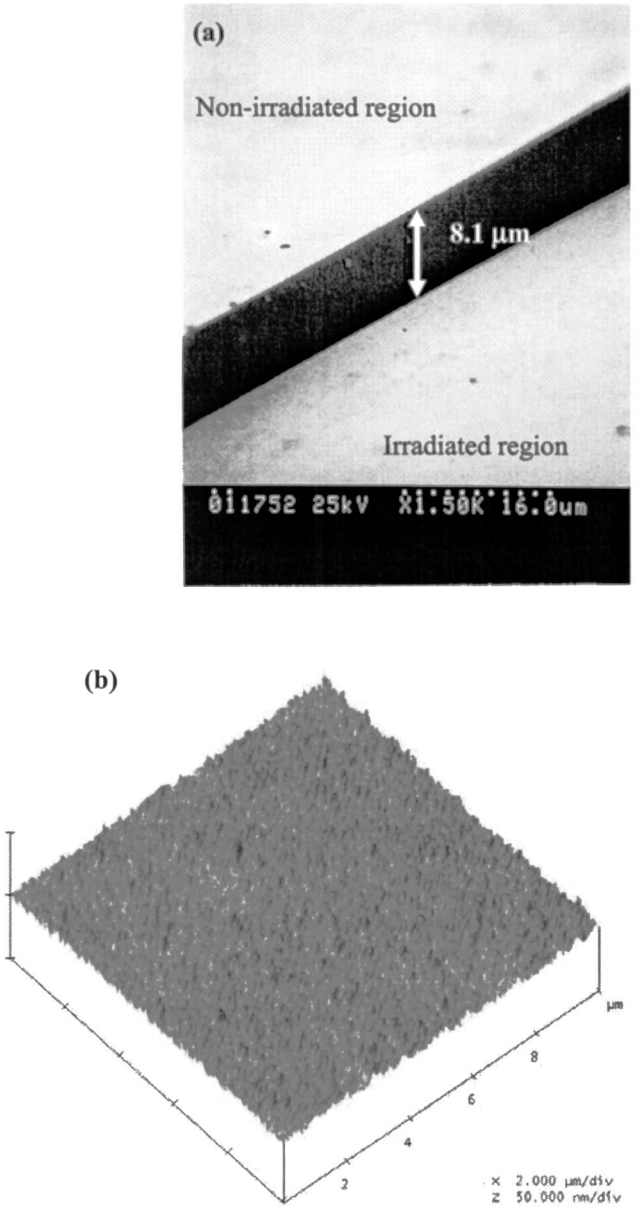

FIG. 2. (a) A SEM image of the rutile surface irradiated with 110-MeV Cu ions to a dose of 8.0×10^{13} cm^{-2} and etched by 20% hydrofluoric acid. The upper left area was covered with a silicon wafer during the irradiation. (b) An AFM image of the etched surface.

soaked in the HF solution for 40 min. A clear 8.1-μm step with a very smooth sidewall can be seen between the irradiated and nonirradiated regions. The bottom surface of the irradiated region also looks very smooth. This smoothness is more clearly manifested by its AFM image shown in Fig. 2(b), where the maximum observable roughness is 2.5 nm.

The rutile (100) crystals were irradiated by Cu ions with an energy of 84.5 MeV to a dose of either 7.0×10^{12}, 1.0×10^{13}, or 5.0×10^{13} cm^{-2}, and then etched with the HF solution. Figure 3(a) shows the etched depth D as a function of the etching time. The kinked solid line represents the result of a least-squares fit to the data for the sample irradiated to a dose of 5.0×10^{13} cm^{-2}. That the values of D start with

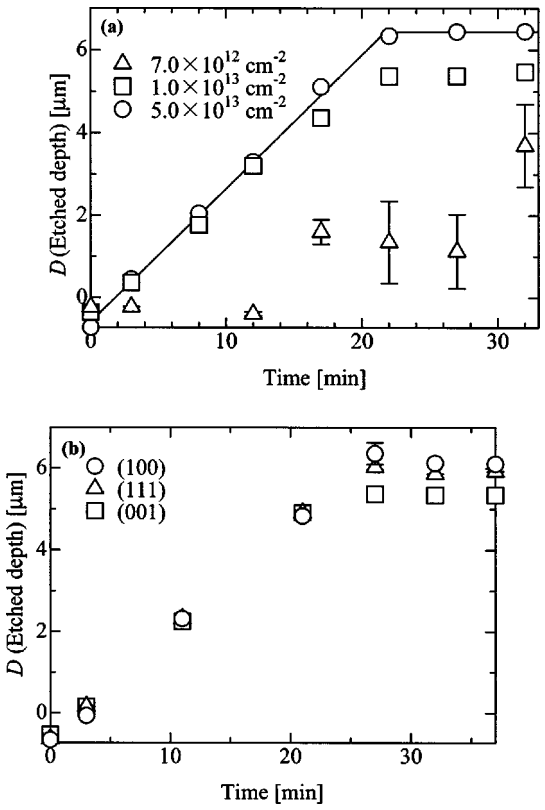

FIG. 3. (a) Relation between the etching time and the etched depth D, observed for the samples irradiated by 84.5-MeV Cu ions to doses of 7.0×10^{12} cm^{-2} (triangles), 1.0×10^{13} cm^{-2} (squares), and 5.0×10^{13} cm^{-2} (circles). The kinked line represents the result of least-squares fit to the data for the sample irradiated to 5.0×10^{13} cm^{-2}. (b) Effect of the surface orientation on the etching property for the samples irradiated to a dose of 5.0×10^{13} cm^{-2}.

negative values corresponds to the volume expansion caused by irradiation. The D value increases linearly to a saturation value D_e of about 5.4 μm for the case of 1.0×10^{13} cm^{-2} and 6.4 μm for 5.0×10^{13} cm^{-2}. The dependence of D on the etching time was also examined for the (111) and (001) crystals irradiated by Cu ions to a dose of 5.0×10^{13} cm^{-2}, and the result is shown in Fig. 3(b). A similar increase in D is seen, although D_e may depend on the surface orientation. Note that the reason of the small difference in D value for the (100) crystal between Figs. 3(a) and 3(b) is that the experiment was repeated to confirm the reproducibility.

As shown in Fig. 3(a), D_e depends on the irradiation dose. Figure 4 shows the change in D_e as a function of the irradiation dose of 84.5-MeV Cu ions. It can be seen that etching becomes possible at doses higher than 5×10^{12} cm^{-2} and that D_e becomes saturated at D_s when the dose exceeds a critical value of about 2×10^{13} cm^{-2}. The values of D_s observed for various ions with different energies are summarized in the rightmost column in Table I. The value of D_s is always around 10 times higher than H, which strongly indicates that the structural change through which the etching becomes possible is closely related to the volume expansion.

Figure 5 shows XRD spectra of the (100) rutile irradiated by the 84.5-MeV Cu ions. Spectrum (i) is for the nonirradi-

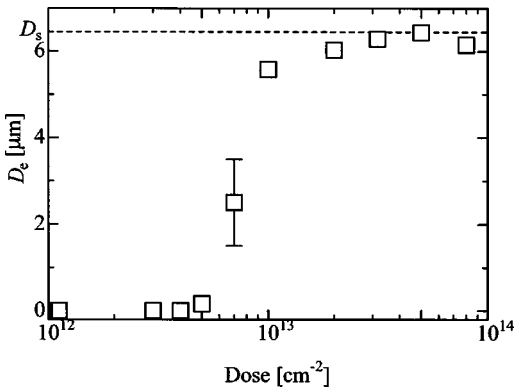

FIG. 4. Change in D_e as a function of irradiated dose of 84.5-MeV Cu ions.

ated sample. Two peaks at 39.2° and 84.3°, to be assigned to the (200) and (400) planes, are seen. Curves (ii), (iii), (iv), and (v) are the spectra obtained in the samples after having been irradiated to respective doses of 1.0×10^{12}, 3.0×10^{12}, 7.0×10^{12}, and 5.0×10^{13} cm^{-2}, while curve (vi) is the one after the sample used to obtain curve (iii) was etched in the HF solution for 30 min. The two XRD peaks become smaller by the ion irradiation. Besides them, new peaks appear at 38.3° and 82.5° in spectrum (iii). They become smaller and move to smaller angles as the irradiation dose increases, and finally disappear in spectrum (v).

In order to observe separate individual latent tracks, the rutile was irradiated by 84.5-MeV Cu ions to a low dose of 1.0×10^{10} cm^{-2} and was observed by HREM. Two white spots located near the upper-left and lower-right corners in Fig. 6(a) are latent tracks. Another HREM image with a

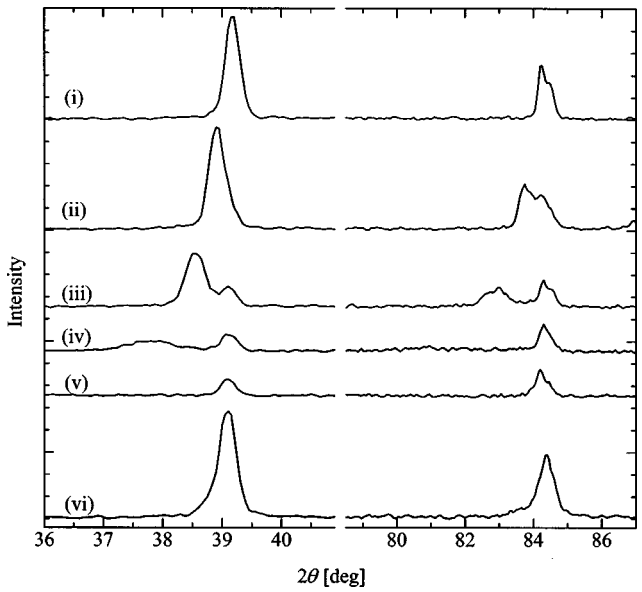

FIG. 5. XRD spectra of the nonirradiated rutile (i), after irradiation of 84.5-MeV Cu ions to doses of 1.0×10^{12} (ii), 3.0×10^{12} (iii), 7.0×10^{12} (iv), and 5.0×10^{13} cm^{-2} (v). Curve (vi) is the spectrum of the sample (iii) after having been etched in HF for 30 min. The peaks at 39.2° and 84.3° are due to the (200) and (400) planes, respectively.

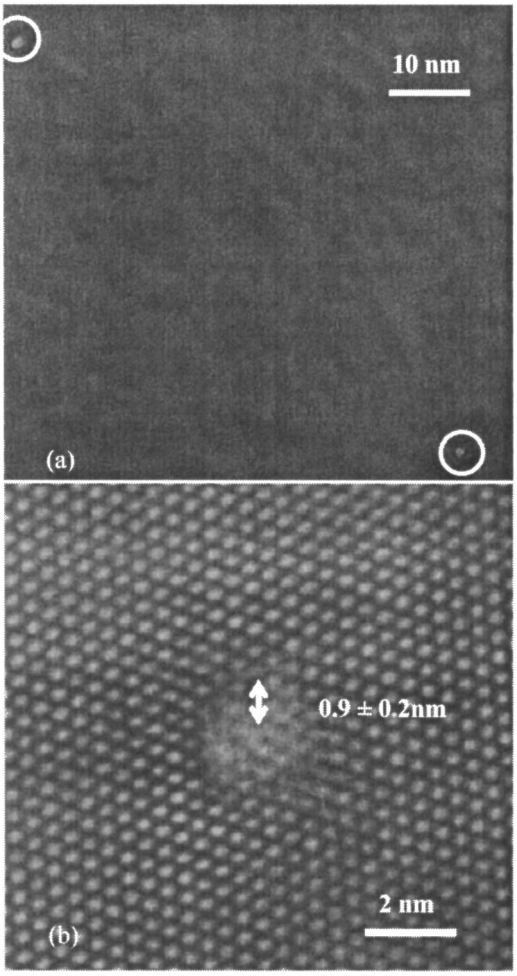

FIG. 6. HERM images of the rutile irradiated by 84.5-MeV Cu ions to a dose of 1.0×10^{10} cm^{-2}. A bright image and a lattice are shown in (a) and (b), respectively.

larger magnification shown in Fig. 6(b) indicates that the latent tracks is of a circular shape with a radius of 0.9 $\pm$0.2 nm and is surrounded by a dark region with a radius of about 1.8 nm.

Figure 7 shows the electronic stopping power S_e calculated by the SRIM 98 code[33] as a function of depth from the sample surface. The solid circle on each curve is plotted so that its value on the x axis corresponds to the value of D_s summarized in Table I. The dotted curves in Fig. 7 imply the regions where etching was observed, while solid curves imply the nonetched regions. It is easily seen that D_s is smaller than the depth at $S_e=0$, where ions are to stop. An important fact is that all the D_e values or the solid circles lie nearly on the solid horizontal line representing the positions where the electronic stopping power becomes 6.2 keV/nm irrespective of the ion species and acceleration energy. It is considered that a threshold electronic stopping power of 6.2 keV/nm is necessary for the ions to make the rutile structure suitable for etching.

The validity of the threshold electronic stopping power is further examined for different ions. As a first step, Ca ions with various energies were irradiated on the rutile crystals to a dose of 8.0×10^{13} cm^{-2}. Then, they were examined by

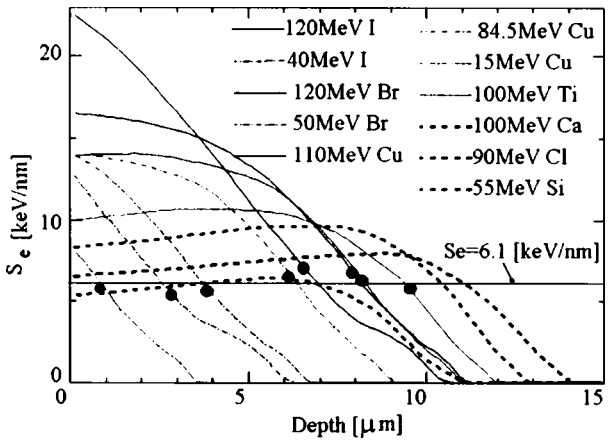

FIG. 7. Calculated electronic stopping power S_e as a function of the depth from the surface. The x-axis values of the solid circles indicate the depths where the etching stopped.

XRD and were etched in the HF solution. Figure 8 shows the obtained XRD spectra for the nonirradiated crystal (a) and for the irradiated crystals at energies of 15.3 MeV (b), 31.9 MeV (c), 50.8 MeV (d), 72.3 MeV (e), and 82.0 MeV (f). Both the intensity of the 39.2° peak and that of the 84.3° peak decrease until 50.8 MeV and then return to their original values. As a surprising result, it was found that the sample surface irradiated by either the 15.3-MeV, 31.9-MeV, or 50.8-MeV ions was etched, while the one irradiated by the 72.3-MeV or 82.0-MeV ions was not.

Furthermore, another surprising result was obtained. Namely, after the crystals were irradiated by the Ca ions with various energies to a dose of 8.0×10^{13} cm^{-2}, they were cut perpendicularly to the surface and immersed in the HF solution. Figure 9 shows a typical cross-sectional SEM image taken for the sample irradiated by the 72.3-MeV ions. The

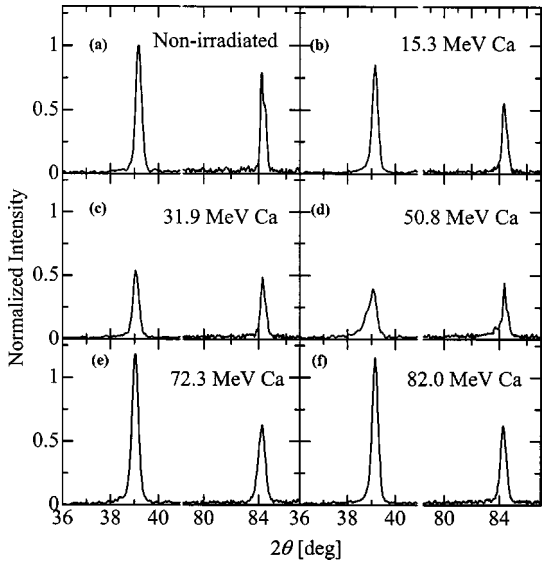

FIG. 8. XRD spectra obtained before and after irradiation of Ca ions to a dose of 8.0×10^{13} cm^{-2}. (a) Before irradiation. (b)–(f) After irradiation of ions with energies of 15.3 MeV (b), 31.9 MeV (c), 50.8 MeV (d), 72.3 MeV (e), and 82.0 MeV (f).

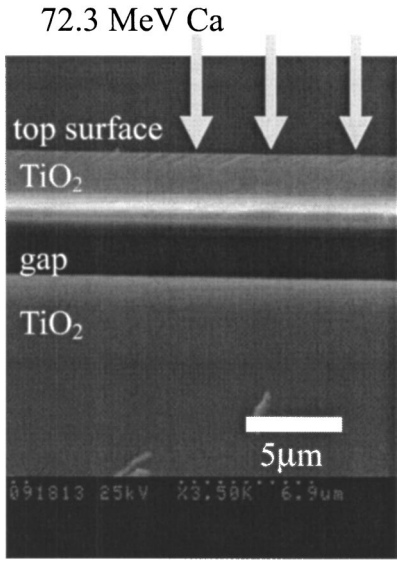

FIG. 9. A cross-sectional SEM image of the sample etched following the irradiation of the 72.3-MeV Ca ions to a dose of 8.0×10^{13} cm^{-2}.

position of the irradiated top surface and the direction of ions are indicated by arrows. The top surface was not etched, while an inside gap or a vacant hollow was created by etching about 4 μm below the surface. Similar inside gaps were always observed if the energy of Ca ions was higher than 72.3 MeV, and the position of the gap became deeper as the energy increased. For example, when the energy was 82.0 MeV, the gap was seen at depths between 5.4 and 7.7 μm from the top surface. Figure 10 shows the electronic stopping power S_e as a function of the depth. The dotted portion of each curve shows the depths where the hollow etching was made. Similar hollow etching was also observed in rutile irradiated by Cl ions with energies of 77.0 MeV and higher to a dose of 1.0×10^{15} cm^{-2}.

IV. DISCUSSION

As shown in Fig. 5, the XRD peaks at 39.2° and 84.3° due to the rutile crystal structure decrease and move to

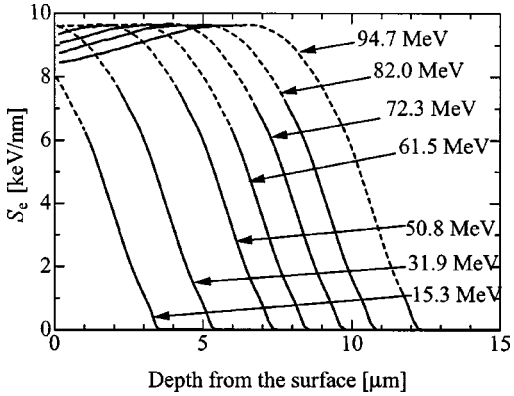

FIG. 10. Calculated values of S_e of Ca ions injected with various energies as a function of the depth from the sample surface. The dotted portion of each curve represents the depths where the hollow etching was made.

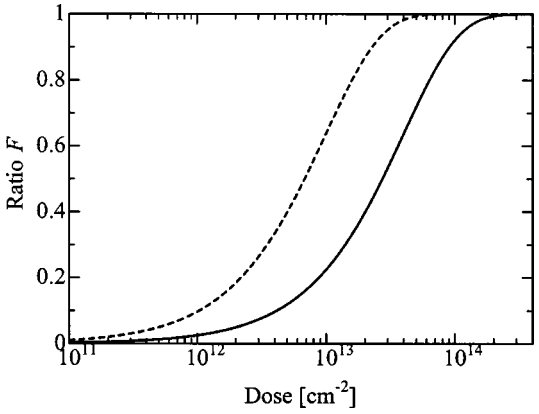

FIG. 11. Change in the ratio F of the area affected by the irradiation of 84.5-MeV Cu ions to the entire sample surface. The solid curve is the result obtained by assuming that the area affected is limited to the amorphous region, while the dotted one is under the assumption that the area includes the surrounding region.

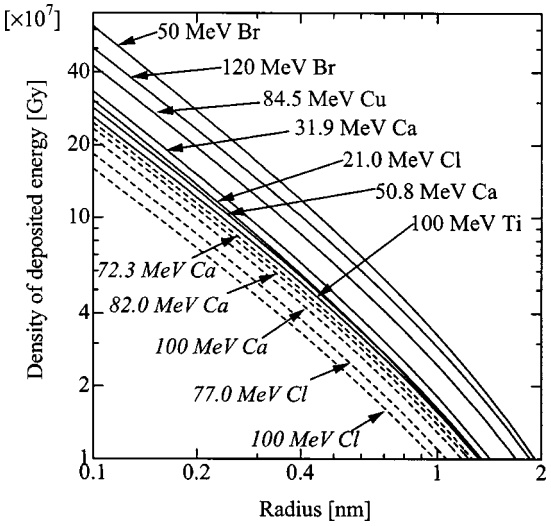

FIG. 12. Radial distribution of energy deposited on the rutile surface as a function of the distance from the ion incident point. Solid curves with roman letters mean that the surface was etched, while dotted ones with italics represent that the inside was etched.

smaller angles by the ion irradiation. According to the Bragg law, peaks at smaller angles are due to a structure with larger lattice constants. Therefore, it is clear that the irradiated layer of the sample became amorphous and increased its volume as evidenced by H shown in Table I. Since rutile has the largest density among TiO_2 polymorphs, it is reasonable that the volume expands as the structure becomes amorphous. As shown by a comparison of spectra (i)–(v) in Fig. 5, the intensities of the crystal peaks scarcely change when the dose exceeds 3.0×10^{12} cm^{-2}. Since the penetration depth of x rays for XRD is much deeper than that of ions,[34] the crystal peaks in curves (iii)–(v) are considered to come from the undamaged rutile beyond the ion penetration depth. Therefore, it was assumed that the samples shown in (iii)–(v) became completely amorphous after having undergone a partly amorphous state. The surrounding dark region in the HREM lattice image in Fig. 6 corresponds to the region where the lattice constant becomes larger.

In order to examine whether the etched region is limited to the amorphous region or covers the surrounding region, the following calculations were performed. In general, the ratio F of the area affected by the ion irradiation to the whole sample surface is known to be expressed by the equation

$$F = 1 - \exp(-A\phi), \tag{1}$$

where A is the area affected by the passage of a single ion and ϕ is the total ion dose.[35] If only the amorphous region is regarded as the affected area, A is estimated from Fig. 6 to be $\pi\times0.9^2$ nm^2 for the 84.5-MeV Cu ion. The solid curve in Fig. 11 shows the change in F as a function of ϕ for the 84.5-MeV Cu ions. If F represents the ratio of the area which can be etched, this result indicates that a dose higher than about 3×10^{14} cm^{-2} is needed for the amorphous area to cover the whole sample surface. This dose is more than one order of magnitude higher than the dose at which the etching started. If a similar calculation is made for the area including the surrounding region with a radius of 1.8 nm, the dashed curve in Fig. 11 is obtained. It is indicated that the region to be etched covers about 50% of the sample surface at the irradiation dose of 7.0×10^{12} cm^{-2}, where the surface etching was really observed in Fig. 4. From these calculations, it is highly probable that the surrounding region as well as the amorphous region can be etched by the HF solution. The fact that the XRD peaks ascribed to the surrounding region also disappear by etching as clearly shown by a comparison between the curves (iii) and (v) in Fig. 5 is in a good agreement with the above assumption. The fact that the etching rate for the dose of 7.0×10^{12} cm^{-2} is widely scattered and is slower than that for higher doses as shown in Fig. 3(a) is also explained by the dotted curve in Fig. 11, which indicates that the etching becomes possible at doses of the order of 10^{12} cm^{-2}.

Next, the mechanism of the inside hollow etching shown in Fig. 9 is discussed. Figure 10 indicates that the hollow etching is not simply understandable by S_e. It has been reported that a slower electron deposits a higher energy density to the target surface than a faster electron.[36] It has been also reported that a faster ion makes a smaller latent track than a slower ion with the same S_e.[37] These reports indicate that the velocity of electrons or ions is another factor besides S_e to decide the deposited energy and the radius of latent tracks. A semiempirical equation based on the Rutherford formula, in which the ion velocity is taken into account, has been developed to calculate the radial distribution of energy deposited on the sample surface around the path of ions.[38] Figure 12 shows calculation results of the radial distribution of energy deposited on a rutile surface around the path of ions as a function of the distance (or radius) from the ion incident point, obtained by assuming the same ion species and energies as those used in the present experiment. Solid curves with roman letters represent the conditions where the rutile surface was etched, while dotted curves with italics represent those where the inside was etched. All the solid curves lie above the dotted ones irrespective of the ion species and energy, which indicates that the energy deposited on the sur-

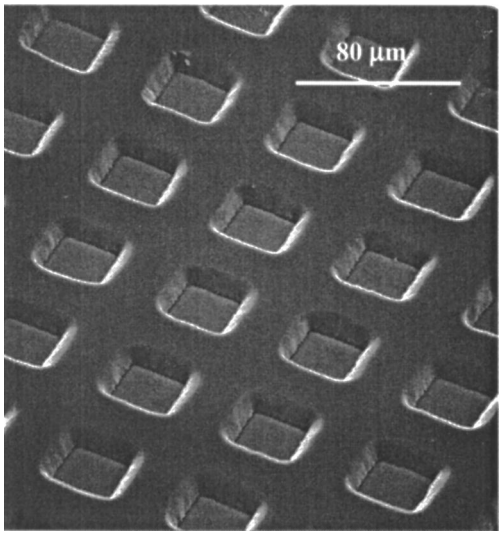

FIG. 13. An SEM image of the etched surface with 20% hydrofluoric acid of the same sample shown in Fig. 1. The sidewall pattern is a replica of that of the holes through which the ions were irradiated.

face by incident ions is a more critical factor to determine whether the irradiated rutile can be etched or not.

Last, applications of the phenomena obtained in the present research are discussed. The sample to which the 120-MeV Br ions were irradiated through the two-dimensional pattern of holes, of which AFM image is shown in Fig. 1, was etched in the HF solution for 40 min and subjected to SEM observation. Figure 13 shows the result. While the bottom surfaces of the etched cavities seem very flat, the sidewalls look as if they were rough. However, this sidewall structure is a replica of the shape of the holes. Therefore, this means that the present combination of ion irradiation and etching has a very precise resolution, capable of being applied as a nanofabrication method. By combining the irradiation of ions with various energies suitable for multilayer inside hollow etching, three-dimensional nanofabrication is also possible.

V. CONCLUSIONS

The structural change induced in rutile TiO_2 single crystals by irradiation of swift heavy ions has been investigated. Through XRD and HREM analyses, it is considered that the latent tracks induced by the passage of ions become amorphous and that the lattice constants in the surrounding area become larger. If the rutile crystal is irradiated by swift heavy ions to a dose higher than the critical value at which the latent tracks and their surrounding areas presumably cover a large portion of the rutile surface, the surface becomes possible to be etched by hydrofluoric acid. When Ti, Cu, Br, or I ions are irradiated, the etching continues to the depth from the surface where the electronic stopping power decays to a threshold value of 6.2 keV/nm, regardless of the ion species. Excepting the above, the surface cannot be etched even if the stopping power exceeds the threshold when the ion is Cl or Ca. However, in this case, a hollow vacancy layer is etched inside the sample. By calculating the radial distribution of energy deposited on the surface by the incident ions, it becomes evident that there is a clear demarcation in the radial energy distribution which determines whether the surface can be etched or not. The bottom and side surfaces of the etched cavities were found to be very smooth in the order of nm. Therefore, combination of irradiation by swift heavy ions with various energies and following etching is believed to be a good processing method to fabricate three-dimensional nanostructures.

ACKNOWLEDGMENTS

This work was supported by the Budget for Nuclear Research approved by the Atomic Energy Commission and also by a Grant-in-Aid for Scientific Research Grant No. (12450132), both from the Ministry of Education, Culture, Sports, Science, and Technology of Japan. The authors express their thanks to T. Sekiguchi in Kagami Memorial Laboratory for Materials Science and Technology, Waseda University for his help.

*Corresponding author. FAX: +81-29-861-2919. Electronic address: k.awazu@aist.go.jp

[1] A. Fujishima and K. Honda, Nature (London) **238**, 37 (1972).
[2] A. Mills and S. Le Hunte, J. Photochem. Photobiol., A **108**, 1 (1997).
[3] H. Liu, H. T. Ma, X. Z. Li, W. Z. Li, M. Wu, and X. H. Bao, Chemosphere **50**, 39 (2003).
[4] R. K. Karn and O. N. Srivastava, Int. J. Hydrogen Energy **24**, 27 (1999).
[5] M. G. Kang, N.-G. Park, Y. J. Park, K. S. Ryu, and S. H. Chang, Sol. Energy Mater. Sol. Cells **75**, 475 (2003).
[6] C. Chaudhari and D. K. Gautam, Opt. Commun. **181**, 61 (2000).
[7] E. M. Yeatman, M. M. Ahmad, O. McCarthy, A. Vannucci, P. Gastaldo, D. Barbier, D. Mongardien, and C. Moronvalle, Opt. Commun. **164**, 19 (1999).
[8] C. Tosello, F. Rossi, S. Ronchin, R. Rolli, G. C. Righini, F. Pozzi, S. Pelli, M. Fossi, E. Moser, M. Montagna, M. Ferrari, C. Duverger, A. Chiappini, and C. De Bernardi, J. Non-Cryst. Solids **284**, 230 (2001).
[9] Z. Jiwei, Y. Tao, Z. Liangying, and Y. Xi, Ceram. Int. **25**, 667 (1999).
[10] T. C. Lu, L. B. Lin, S. Y. Wu, J. Chen, and Y. Y. Ahang, Nucl. Instrum. Methods Phys. Res. B **191**, 236 (2002).
[11] D. F. Sievenpiper and E. Yablonovitch, Phys. Rev. Lett. **80**, 2829 (1998).
[12] W. M. Robertson and G. Arjavalingam, Phys. Rev. Lett. **68**, 2023 (1992).
[13] V. V. Poborchii, T. Tada, and T. Kanayama, Appl. Phys. Lett. **75**, 3276 (1999).
[14] E. Yablonovitch, Phys. Rev. Lett. **58**, 2059 (1987).
[15] S.-Y. Lin, V. M. Hietala, L. Wang, and E. D. Jones, Opt. Lett. **21**, 1771 (1996).
[16] H. Kosaka, T. Kawashima, A. Tomita, M. Notomi, T. Tamamura, T. Sato, and S. Kawakami, J. Lightwave Technol. **17**, 2032

(1999).
[17] A. Mekis, J. C. Chen, I. Kurland, S. Fan, P. R. Villeneuve, and J. D. Joannopoulos, Phys. Rev. Lett. **77**, 3787 (1996).
[18] P. R. Villeneuve, S. Fan, J. D. Joannopoulos, K.-Y. Lim, G. S. Petrich, L. A. Kolodziejski, and R. Reif, Appl. Phys. Lett. **67**, 167 (1995).
[19] A. Birner, A.-P. Li, F. Müller, U. Gösele, P. Kramper, V. Sandoghdar, J. Mlynek, K. Busch, and V. Lehmann, Mater. Sci. Semicond. Process. **3**, 487 (2000).
[20] C. Weisbuch, H. Benisty, M. Rattier, C. J. M. Smith, and T. F. Krauss, Synth. Met. **116**, 449 (2001).
[21] R. H. Klazes, M. H. L. M. van der Broek, J. Bezemer, and S. Raderlaar, Philos. Mag. B **45**, 377 (1982).
[22] I. H. Malitson, J. Opt. Soc. Am. **55**, 1205 (1965).
[23] D. Mergel, Thin Solid Films **397**, 216 (2001).
[24] S. Yamazaki, N. Hata, T. Yoshida, H. Oheda, A. Matsuda, H. Okushi, and K. Tanaka, J. Phys. (Paris), Colloq. **42**, C4-297 (1981).
[25] C. Cardinaud, M.-C. Peignon, and P.-Y. Tessier, Appl. Surf. Sci. **164**, 72 (2000).
[26] S. Norasetthekul, P. Y. Park, K. H. Baik, K. P. Lee, J. H. Shin, B. S. Jeong, V. Shishodia, E. S. Lambers, D. P. Norton, and S. J. Pearton, Appl. Surf. Sci. **185**, 27 (2001).
[27] S. Shimada, K. Miyazawa, and M. Kuwabara, Jpn. J. Appl. Phys., Part 2 **41**, L291 (2002).
[28] M. Lanata, M. Cherchi, A. Zappettini, S. M. Pietralunga, and M. Martinelli, Opt. Mater. (Amsterdam, Neth.) **17**, 11 (2001).
[29] W. Hu, H. Li, B. Cheng, J. Yang, Z. Li, J. Xu, and D. Zhang, Opt. Lett. **20**, 964 (1995).
[30] K. Awazu, S. Ishii, K. Shima, S. Roorda, and J. L. Brebner, Phys. Rev. B **62**, 3689 (2000).
[31] G. Fiedler, J. Aschenbach, W. Otto, T. Rautenberg, U. Steinhauser, and G. Siegert, Nucl. Instrum. Methods **147**, 35 (1977).
[32] G. Bonfiglioli, A. Ferro, and A. Monjoni, J. Appl. Phys. **32**, 2499 (1961).
[33] J. F. Ziegler, J. P. Biersack, and U. Littmark, *The Stopping Power and Ranges of Ions in Matter* (Pergamon, New York, 1985), Vol. I.
[34] http://www-cxro.lbl.gov/
[35] M. Toulemonde, E. Balanzat, S. Bouffard, J. J. Grob, M. Hage-Ali, and J. P. Stoquert, Nucl. Instrum. Methods Phys. Res. B **46**, 64 (1990).
[36] R. Kats and E. J. Kobetich, Phys. Rev. **186**, 344 (1969).
[37] A. Meftah, F. Brisard, J. M. Costantini, M. Hage-Ali, J. P. Stoquert, F. Studer, and M. Toulemonde, Phys. Rev. B **48**, 920 (1993).
[38] M. P. R. Waligorski, R. N. Hamm, and R. Kats, Nucl. Tracks Radiat. Meas. **11**, 309 (1986).